Structural basis for Nirmatrelvir in vitro efficacy against the Omicron variant of SARS-CoV-2

Greasley, Samantha E[1], Noell, Stephen[2], Plotnikova, Olga[2], Ferre, RoseAnn[1], Liu, Wei[1], Bolanos, Ben[1], Fennell, Kimberly[2], Nicki, Jennifer[2], Craig, Tim[2], Zhu, Yuao[3],Stewart, Al E[1], Steppan, Claire M*[2]

[1] Pfizer Worldwide Research, Development & Medical, La Jolla, CA, 92037, USA.

[2] Pfizer Worldwide Research, Development & Medical, Groton, CT, 06340, USA.

[3]Pfizer Worldwide Research, Development & Medical, Pearl River, NY, 10965,USA

*Corresponding Author Email: claire.m.steppan@pfizer.com

Keywords: PF-07321332, nirmatrelvir, 3CLpro, Mpro, Ki, VOC, crystal structure, Omicron

Abstract

The COVID-19 pandemic continues to be a public health threat with emerging variants of SARS-CoV-2. Nirmatrelvir (PF-07321332) is a reversible, covalent inhibitor targeting the main protease (M^{pro}) of SARS-CoV-2 and the active protease inhibitor in PAXLOVID™ (nirmatrelvir tablets and ritonavir tablets). One of the predominant SARS-CoV-2 variants emerging is the B.1.1.529 Omicron harboring a mutation at amino acid position 132 in the M^{pro} changing a proline to a histidine (P132H). In vitro biochemical enzymatic assay characterization of the enzyme kinetics of the Omicron M^{pro} (P132H) demonstrate that it is catalytically comparable to wildtype and that nirmatrelvir has similar potency against both wildtype and Omicron (P132H) M^{pro} with Ki of 0.933nM (wildtype) and 0.635nM (P132H) each, respectively. This observation is reinforced by our structural determination of nirmatrelvir bound to the omicron M^{pro} at 1.63Å resolution. These *in vitro* data suggest that PAXLOVID has the potential to maintain plasma concentrations of nirmatrelvir many-fold times higher than the amount required to stop the SARS-CoV-2 variant Omicron from replicating in cells.

Main Text

New viral infectious diseases are emerging and have caused major public health crises in recent years. Reported examples in the last 20 years include severe acute respiratory syndrome coronavirus (SARS-CoV), H1N1 influenza, the Middle East respiratory syndrome coronavirus (MERS-CoV), Ebola virus disease (EVD), and Zika virus (1). The world continues to grapple with a global pandemic caused by a novel coronavirus, SARS-CoV-2 that was initially reported to the World Health Organization (WHO) on December 31, 2019 (2). Later, WHO designated this virus as the severe acute respiratory syndrome coronavirus-2 (SARS-CoV-2) owing to its similarity with the previous SARS-CoV (3). Then at the end of January, WHO declared this viral outbreak as a public health emergency of international concern (4), and subsequently characterized it as a pandemic.

SARS-CoV-2 is a highly infectious, ribonucleic acid (RNA) beta coronavirus that can be life-threatening in serious cases. While effective COVID-19 vaccines have been developed, a significant number of people have yet to be vaccinated -either because of pre-existing medical conditions, vaccination hesitancy or challenges with access. Therefore, therapeutics are needed to effectively combat coronavirus disease 2019 (COVID-19). (5)

The SARS-CoV-2 genome encodestwo polyproteins (pp1a and pp1ab) and four structural proteins (5). The polyproteins are cleaved by the critical SARS-CoV-2 main protease (M^{pro}, also referred to as 3CL protease) at eleven different sites to yield shorter, non-structural proteins vital to viral replication (5). We have previously reported on the discovery and antiviral efficacy of nirmatrelvir (PF-07321332), an orally bioavailable SARS-CoV-2-M^{pro} inhibitor with in vitro pan-human coronavirus antiviral activity with excellent off-target selectivity and in vivo safety profiles (5). Nirmatrelvir has demonstrated oral activity in a mouse-adapted SARS-CoV-2 model and has achieved oral plasma concentrations that exceed the in vitro antiviral cell potency, in a phase I clinical trial in healthy subjects (5). With Omicron being a dominant variant of concern, we evaluated the biochemical potency of nirmatrelvir against the M^{pro} harboring a mutation at P132 which exists in Omicron. We demonstrate that nirmatrelvir has a comparable potency against the Omicron protease relative to wildtype (M^{pro} from the original Washington variant (USA-WA1/2020). This observation is reinforced by our structural determination of nirmatrelvir bound to the omicron protease at 1.63 Å resolution (Figure 2).

Full-length wildtype SARS-CoV-2 M^{pro} and Omicron P132H were expressed and purified to near homogeneity as demonstrated by a singular protein peak with a confirmed intact mass of 33.8 kDa for a fully authentic form of each protein. (Figure 1A). Briefly, the wild type SARS-Cov2-M^{pro} construct was designed based on Su et al 2020 (6). An additional N-terminal PreScission protease cleavage site was inserted between GST and the self-cleavage site. Site directed mutagenesis was performed to make the P132H variant. The resulting plasmid was then transformed into BL21 (DE3) cells for protein expression. One liter of LB media was inoculated with 30mL of overnight culture and grown at 37°C until an OD_{600} of 0.6 was reached. The culture was induced using a final concentration of 0.2 mM IPTG and harvested 1 hour post induction. Cells were lysed in 20 mM Tris pH 8.0 buffer containing 500 mM NaCl, 10% glycerol, 0.2 mM TCEP with a microfluidizer, and the mixture was clarified by centrifugation at 15000 x g. The resulting supernatant was purified by a Ni-affinity column using a step gradient, followed by C-terminal His-tag cleavage with PreScission protease, and a secondary Ni-affinity purification to remove non-cleaved M^{pro} and PreScission protease. A final and size exclusion chromatography step showed the M^{pro} P132H protein to be nearly 100% pure (Figure 1B).

An established M^{pro} fluorescence resonance energy transfer (FRET)- based cleavage assay was used to determine enzyme catalytic activity by monitoring initial velocities of the proteolytic activities at varying substrate (SARS canonical peptide) concentrations (5,7,8) (Figure 1C). The turnover number (kcat) was determined to be 0.41 ± 0.144 s^{-1} for the wildtype M^{pro} and 0.39 ± 0.152 s^{-1} for the P132H M^{pro} omicron variant. Additionally, the Michaelis constants (Km) were comparable for both WT and P132H with values of 23.4 and 25.5 mM, respectively. The catalytic efficiencies (kcat/Km) of the P132H variant (22691 $S^{-1}M^{-1}$) is similar to wildtype M^{pro} (22411$S^{-1}M^{-1}$). These data suggest that the Omicron variant M^{pro} exhibits comparable enzymatic properties as compared to wildtype M^{pro}. Next, we evaluated the ability of nirmatrelvir to inhibit both

wildtype and P132H M^{pro} activity (Figure 1D). Nirmatrelvir potently inhibited both wildtype with a mean Ki of 0.93 nM and the mutated enzyme containing the P132H substitution with a mean Ki of 0.64 nM (Table 1). A comparison of the P132H mutated enzyme potency to that of wildtype M^{pro} by t-Test using the log of individual Ki values with one tail and un-equal variance determined a p-value of 0.07 indicating that the Ki values are not statistically different. These observations are consistent with recently reported biochemical characterization with similar kcat/Km and nirmatrelvir potency values (9). Nirmatrelvir also appears to retain its in vitro antiviral efficacy against Omicron relative to wildtype (10).

The crystal structure of SARS-CoV-2 Omicron P132H M^{pro} bound to nirmatrelvir was determined at 1.63Å. Apo crystals of SARS-CoV-2 Omicron P132H M^{pro} were obtained via vapor diffusion in sitting drops using MRC-Maxi (Swissci) plates where protein, at 7.30 mg/ml, was mixed 1:1 with well solution containing 20% w/v polyethylene glycol (PEG) 3350 and 0.12 M sodium sulfate. Plates were incubated at 21°C and crystals grew in under 24 hours. PF-07321332 (1 mM final concentration) was added directly to the crystallization drop and allowed to soak into the apo crystals for 3 hours at 30 °C. Soaked crystals were then passed through a cryoprotectant consisting of well buffer containing 20% ethylene glycol, and flash cooled in liquid nitrogen in preparation for data collection.

X-ray diffraction data were collected at -173°C at IMCA-CAT 17-ID beamline (11, 12) of the Advanced Photon Source (APS) at Argonne National Labs (13) and the structure was determined by difference Fourier and refined using the anisotropically scaled data as described previously for wildtype SARS-CoV-2-M^{pro} in complex with PF-07321332 (5). Diffraction data processing and model refinement statistics for the mutant M^{pro} are given in Table 2.

Comparison of the SARS-CoV-2 Omicron P132H M^{pro} crystal structure to the wildtype M^{pro}, the structure of which was reported in detail previously (5,14), shows that the binding mode of nirmatrelvir is the same in both structures as shown in Figure 2a. Indeed, Pro 132 is located approximately 16.5Å (Cα-Pro132 to Cα-Glu166) from the PF-07321332 binding pocket. The protein structure surrounding the mutation, P132H, remains structurally unchanged with the except of the side change conformation of Glu 240 which adopts a different rotomer to avoid a potential clash with the histadine side chain. In addition, a water molecule (Wat 1, Figure 2b) observed in the wildtype M^{pro} structure is displaced by the side chain of His 132.

To provide an extended SARS-Cov-2 M^{pro} structural assessment, the solution-phase structural dynamics of P132H and wildtype SARS-Cov2 M^{pro} (10 μM, 25 mM Tris pH=7.2, 150 mM NaCl) were individually profiled using HDX-MS. Native protein was deuterium exchanged at four time points (15s, 1m, 10m, 1h), and subsequently digested with two protease columns (Protease XIII/Pepsin (NovaBioAssays) and Nepenthesin-1 (AffiPro) to generate deuterated peptides for LC-MS analysis. A total of 405 WT peptides were identified (Table 3) on the Fusion Lumos OrbiTrap mass spectrometer (mass tolerance <5 ppm) using Proteome Discoverer 2.2.0 software (Thermo Fisher Scientific). Residual plot (Figure 2c) comparing WT and P132H deuterium uptake profiles (HD Examiner 3.3.0 software, Sierra Analytics) revealed no significance differences (± 6% deuterium) in the backbone dynamics of P132H from wild-type SARS-Cov-2 M^{pro}. These results provided the assurance that the P132H mutation alone did not produce a significant shift from wild-type solution-phase backbone conformational dynamics.

The emergence of naturally occurring SARS-CoV-2 variants exemplify its ability to mutate and signify the continued potential for this pandemic to be problematic. We need to constantly surveil these emerging variants of concern to understand the efficacy of current therapies. Studies described here demonstrate the in vitro inhibitory activity of nirmatrelvir against the Omicron variant M^{pro} and indicate the structural basis for retention of in vitro potency against this mutant protein. They also inform the methods for assessing activity against subsequent variants possessing mutations in the M^{pro} protein.

Table 1:

Potency of PF-07321332 for Inhibiting the SARS-CoV2 Mutant M^{pro} Activity in a FRET Assay

Mutant Enzyme	Ki (nM) GeoMean	Ki (nM) lower 95% CI	Ki (nM) upper 95%	n	P-value[b] to Wild Type Ki
P132H	0.635	0.179	2.25	4[a]	0.074
wild type	0.933	0.471	1.85	9[a]	NA

a. The n value represents the number of Ki values used to determine the geomean and CI which is lower than the experiment count due to censoring, ie experimental values that are < are excluded from GeoMean calculation.
b. p-value calculated as a t-test statistic for log Ki values compared to wild type.

Table 2:

Data Statistics	
PDB entry ID	xxxx
Wavelength (Å)	1.0
Resolution	112.84 – 1.63
Space group	$P2_1$
Unit cell dimensions [Å]	a = 45.4, b = 53.8, c = 115.5
Unit cell dimensions [°]	$\alpha = \gamma = 90.0$, $\beta = 102.4$
Total number of reflections[a]	178785 (6869)
Unique reflections[a]	53153(2659)
Multiplicity[a]	3.4(2.6)

Completeness (%), spherical[a]	78.0 (18.9)
Completeness (%), ellipsoidal[a]	92.8 (53.2)
Mean $I/\sigma(I)$[a]	11.5 (1.4)
R_{merge}[b]	0.056 (0.607)
R_{pim}[c]	0.035 (0.453)
$CC_{1/2d}$	0.999 (0.635)
Refinement Statistics	
Reflections used	53153
Reflections used for R_{free}	2620
R_{cryst} [e]	0.211
R_{free}	0.250
Ramachandran Plot	
Favoured regions (%)	95.0
Allowed Regions (%)	4.5
Outlier regions (%)	0.5

[a] Numbers in parentheses refer to the highest resolution shell

[b] $R_{merge} = \sum_{hkl}\sum_{i=1}^{n} | I_i(hkl) - \bar{I}(hkl) | / \sum_{hkl}\sum_{i=1}^{n} I_i(hkl)$

[c] $R_{pim} = \sum_{hkl}\sqrt{1/(n-1)}\ \sum_{i=1}^{n} | I_i(hkl) - \bar{I}(hkl) / \sum_{hkl}\sum_{i=1}^{n} I_i(hkl)$ (15)

[d] $CC_{1/2}$ = xxx as defined by Karplus and Diederichs (16)

[e] $R_{cryst} = \sum_{hkl} | F_o(hkl) - F_c(hkl) | \sum_{hkl} | F_o(hkl) |$, where F_o and F_c are the observed and calculated structure factors, respectively.

R_{free} is the same as R_{cryst}, but for 5% of the data randomly omitted from refinement. (17)

Table 3

SARS-CoV-2 Sequence analysis (Wild Type and P132H M^{pro})		
Data Set	SARS2_WT (control)	SARS2_P132H
HDX reaction details	4C	4C
HDX time course (sec)	15, 60, 360, 3600	15, 60, 360, 3600
# of peptides	405	387
Sequence coverage	100.00%	100.00%
Average peptide length / Redundancy	17.24 / 22.82	17.29 / 21.86
Replicates	4	4
Repeatability (avg. stddev of #D)	0.1123	0.12
Significant differences in HDX (delta HDX > X D - 95% CI)	n/a	0.3123 D

Figures:

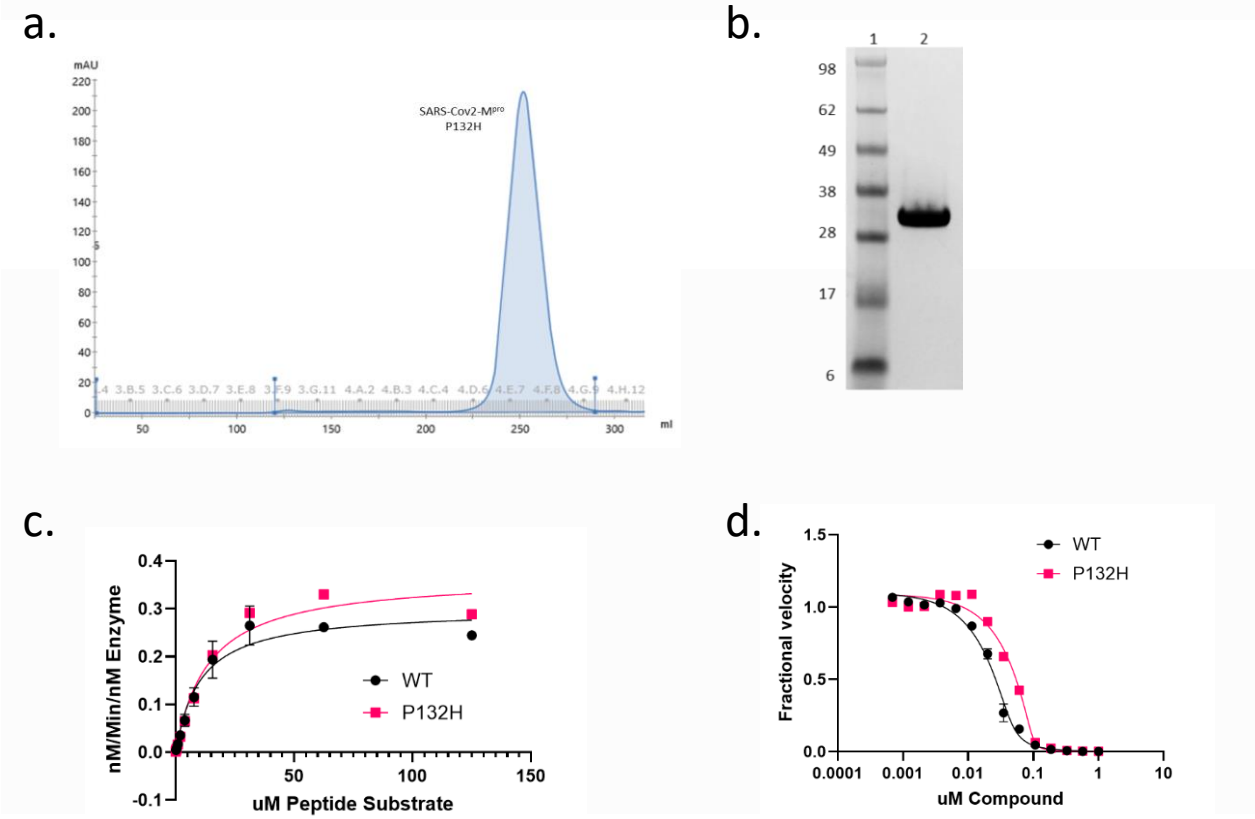

Figure 1.

Purification and characterization of SARS-Cov2-M^{pro} P132H. (a) SEC purification profile using a HiLoad Superdex 200 26/60 column of SARS-CoV-2-M^{pro} (b) SDS-PAGE analysis: Lane 1, Marker; Lane 2, SARS-Cov2-M^{pro} P132H variant (c) Enzyme Kinetics of M^{pro}: The rate of cleavage of the FRET peptide substrate in the presence of 60nM M^{PRO} is monitored by increase in fluorescence over time with the fluorescent signal being converted to nM substrate cleaved by use of a standard curve generated from cleaved substrate. The data was then normalized to the amount of enzyme used in the experiment. (d) Enzyme Inhibition of M^{pro}: M^{pro} activity is monitored in the presence of increasing concentrations of nirmatrelvir with Ki values calculated using the Morrison equation to fit the data.

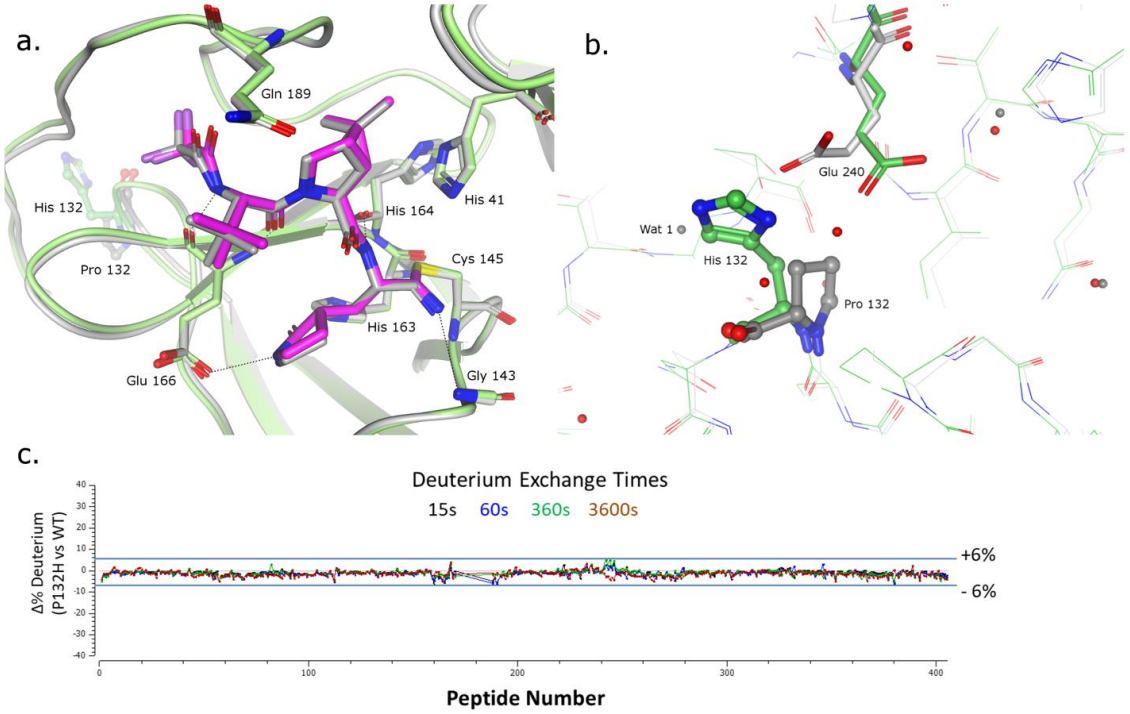

Figure 2.

Structural Characterization of nirmatrelvir bound to SARS-Cov-2-M^{pro} P132H. (a) Superposition of the x-ray crystal structures of nirmatrelvir bound to SARS-Cov-2-M^{pro} P132H (in magenta and green) and wildtype SARS-CoV-2-M^{pro} (grey). Key interactions are indicated via dashed lines. (b) Residues surrounding Proline 132 (in ball & stick representation) (c) Residual deuterium exchange plot indicates no significant differential uptake between wild-type and P132H SARS-CoV-2-M^{pro}.

Acknowledgements: We thank Mark Noe, Gretchen Dean, Jake Wasserman, Annaliesa Anderson and Charlotte Allerton for critical reading of the manuscript and leadership.

Competing Interest Declaration: All authors are employees of Pfizer, Inc and may hold or own shares of stock.

Author Information:

Samantha E Greasley, ORCID, 0000-0002-7978-6477

Stephen Noell, ORCID, 0000-0003-3054-2575

Olga Plotnikova, ORCID, 0000-0002-2513-7287

RoseAnn Ferre, ORCID, 0000-0001-7462-1879

Wei Liu, ORCID, 0000-0002-8541-4928

Ben Bolanos, ORCID, 0000-0003-1171-057X

Kimberly Fennell, ORCID, 0000-0002-1687-5237

Jennifer Nicki, ORCID, 0000-0002-5440-2991

Tim Craig, ORCID, 0000-0002-4625-444X

Yuao Zhu, ORCID, 0000-0002-4129-0599

Claire Steppan, ORCID, 0000-0002-2609-7707

References:

1. Majumder, J., Minko, T. Recent Developments on Therapeutic and Diagnostic Approaches for COVID-19. *AAPS J* **23,** 14 (2021). https://doi.org/10.1208/s12248-020-00532-2

2. Zhou P, Yang XL, Wang XG, et al. A pneumonia outbreak associated with a new coronavirus of probable bat origin. Nature 2020;579(7798) (03):270-3.v DOI: 10.1038/s41586-020-2012-7

3. World Health Organization. (2020). Novel Coronavirus (2019-nCoV): situation report, 1. World Health Organization. https://apps.who.int/iris/handle/10665/330760

4. Coronaviridae Study Group of the International Committee on Taxonomy of Viruses. The species Severe acute respiratory syndrome-related coronavirus: classifying 2019-nCoV and naming it SARS-CoV-2. Nat Microbiol **5,** 536–544 (2020). https://doi.org/10.1038/s41564-020-0695-z.

5. Owen, D. Allerton, C., Anderson, A. An oral SARS-CoV-2 Mpro inhibitor clinical candidate for the treatment of COVID-19. Science. 2 Nov 2021. Vol 374, Issue 6575. pp. 1586-1593. DOI: 10.1126/science.abl4784

6. Su, Hx., Yao, S., Zhao, Wf. et al. Anti-SARS-CoV-2 activities in vitro of Shuanghuanglian preparations and bioactive ingredients. Acta Pharmacol Sin 41, 1167–1177 (2020). https://doi.org/10.1038/s41401-020-0483-6

7. Boras, B., Jones, R.M., Anson, B.J. et al. Preclinical characterization of an intravenous coronavirus 3CL protease inhibitor for the potential treatment of COVID19. Nat Commun 12, 6055 (2021). https://doi.org/10.1038/s41467-021-26239-2.

8. Hoffman, R., Kania, R, Brothers, M., et al, Discovery of ketone-based covalent inhibitors of coronavirus 3CL proteases for the potential therapeutic treatment of COVID-19. J. Med. Chem. 63, 12725-12747 (2020). https://doi10.1021/acs.jmedchem.0c01063

9. Ullrich, s., Ekanayake, B., Otting, G, et al. Main protease mutants of SARS-CoV-2 variants remain susceptible to nirmatrelvir (PF-07321332). bioRXiv 04January2022 (preprint not yet peer reviewed). Doi**:** https://doi.org/10.1101/2021.11.28.470226

10. Vangeel, L., De Jonghe, S., Maes, P. et al., Remdesivir, Molnupiravir and Nirmatrelvir remain active against SARS-CoV-2 Omicron and other variants of concern**.** bioRxiv 28December2021 (preprint, not yet peer reviewed) https://doi.org/10.1101/2021.12.27.474275

11. Use of the IMCA-CAT beamline 17-ID (or 17-BM) at the Advanced Photon Source was supported by the companies of the Industrial Macromolecular Crystallography Association through a contract with Hauptman-Woodward Medical Research Institute.

12.This research used resources at the Industrial Macromolecular Crystallography Association Collaborative Access Team (IMCA-CAT) beamline 17-ID, supported by the companies of the Industrial Macromolecular Crystallography Association through a contract with Hauptman-Woodward Medical Research Institute.

13. This research used resources of the Advanced Photon Source, a U.S. Department of Energy (DOE) Office of Science User Facility operated for the DOE Office of Science by Argonne National Laboratory under Contract No. DE-AC02-06CH11357.

14. Li, j., Lin, C., Zhou, X., et al. Structural basis of main proteases of coronavirus bound to drug candidate PF-07321332. bioRxiv. 08November2021. (preprint, not yet peer reviewed). doi: https://doi.org/10.1101/2021.11.05.467529

15. Weiss, M, Hilgenfeld, R. On the use of the merging R factor as a quality indicator for X-ray data. J. Appl. Crystallogr. 30, 203-205 (1997). doi: Doi 10.1107/S0021889897003907

16. Karplus, P., Diederichs,K. Linking crystallographic model and data quality. Science 336, 1030-1033 (2012). doi: 10.1126/science.1218231

17. Brünger, A. in Methods in Enzymology, C. W. Carter, Jr., R. M. Sweet, Eds. (Academic Press, 1997), vol. 277, chap. 19. doi: 10.1016/s0076-6879(97)77021-6